Finite Element Analysis on Burst Pressure of Steel Pipes with Corrosion Defects

<u>N.A.Alang</u>[1,*], N.A.Razak[1], K.A.Shafie'[1], A.Sulaiman[1]

[1] Corrosion and Fracture Focus Group, Faculty of Mechanical Engineering, University Malaysia Pahang, Malaysia.
* Corresponding author: azuan@ump.edu.my

Abstract   The effect of metal loses due to corrosion on burst pressure of API X42 steel pipes was studied using nonlinear finite element (FE) method. The nonlinear finite element method coupled with stress modified critical strain (SMCS) model was used to predict the failure of the pipes. In this paper, the corrosion defects were simplified to rectangular shape. The procedure in determining the SMCS model parameters from tensile bars was systematically discussed. The effect of defects length, depth and width was investigated. The burst pressure estimated was then compared to available design codes of corroded pipelines. For validation, the results of burst pressure from FE were compared to experimental data. The depth of corrosion defects appears as the most influential parameter that affects the burst pressure of the pipes.

Keywords   Burst Pressure, Corrosion Defects, Stress Modified Critical Strain, Stress Triaxiality

1. Introduction

In petrochemical industry, pipelines play an important role in transporting crude oil and gas. As in service duration increases, the pipelines are affected by corrosion mechanism which leads to fatal accident. Corrosions can occur in both internal and external surfaces of the pipelines. In general, corrosion would cause metal loss which lead to reduction of pipe thickness and consequently decreases its strength. The probability of pipe to burst then will increase. Therefore, failure due to corrosion defects has been a major concern in maintaining pipeline integrity [1]. There are several design codes used in practice to evaluate the remaining strength of corroded pipelines such as American Society of Mechanical Engineer (ASME) B31G [2], modified ASME B31G [2] and DNV-RP-F101 [3] codes. These codes were developed many years ago and used throughout the industry. ASME B31G and modified ASME B31G simplify a short longitudinal corrosion defect as a parabolic curve whereas long corrosion defect can be simplified to a rectangular shape. According to ASME B31G and DNV-RP-F101 codes, the failure of corroded pipelines is controlled by the defect size as well as the flow stress of the material. The DNV-RP-F101 code can be applied for both defect subjected to internal pressure loading only or internal pressure loading combined with longitudinal compressive stresses. However, the ASME B31G is limited to defect subjected to internal pressure only. DNV-RP-F101 design code equations also include the assessment of single and interacting defects and complex shaped defects. The input parameter of these codes include outer diameter of the pipe, D, wall thickness, t, yield strength of the material, σ_y or ultimate tensile strength, σ_u, the length of the defect, L and defect depth, d. The width, w was considered to have less effect on strength of corroded pipe and therefore this factor was avoided in all assessment equations [4]. The equations used to calculate the burst pressure, P_b based on these codes are expressed as:

$$P_b = \frac{2ts_f}{D}$$

(1)

For ASME B31G:

$$S_f = 1.1\sigma_y \left[\frac{1 - \frac{2}{3}\left(\frac{d}{t}\right)}{1 - \frac{2}{3}\left(\frac{d}{t}\right)/M} \right]; \quad M = (1 - 0.8\frac{L^2}{Dt})^{0.5}$$

(2)

For Modified ASME B31G:

$$S_f = (\sigma_y + 69) \left[\frac{1 - 0.85\left(\frac{d}{t}\right)}{1 - 0.85\left(\frac{d}{t}\right)/M} \right]; \quad M = \left[1 + 0.6275\frac{L^2}{Dt} - 0.003375\left(\frac{L^2}{Dt}\right)^2 \right]^{0.5}$$

(3)

For DNV-RP-F101:

$$S_f = (\sigma_y + 69) \left[\frac{1 - 0.85\left(\frac{d}{t}\right)}{1 - 0.85\left(\frac{d}{t}\right)/M} \right]; \quad M = \left[1 + 0.31\frac{L^2}{Dt} \right]^{0.5}$$

(4)

where *M* represents as bulging stress magnification factor.

A numbers of researchers [5-7] have studied the remaining strength of pipelines with corrosion defect using FE method together with stress based failure criterion and used to predict failure in the damage pipe. However, this leads to conservative results because stress based failure criterion relies on flow stress of the materials only. Other methods use strain based failure criterion including Gurson–Tvergaard–Needleman (GTN) model [8], void growth model (VGM) [9], continuum damage model (CDM) [10] and SMCS model [11]. However, a few issues need to be resolved in practical applications of these methods. For example, GTN models consist of relatively high number of parameters compare to SMCS and VGM models [12]. These GTN parameters are difficult to identify and calibrate which require a large number of FE and experimental work.

Oh et al [13] recently developed the SMCS model based on local criteria for API X65. The model was used to predict the burst pressure of pipes with gouge and corrosion defects. The study is limited to API X65 steel material and pipe outer diameter of 762 mm. The accuracy and validity of the model is well discussed and acceptable in wide range of defect geometries. Mathematically, SMCS is evaluated by Eq. (5) through Eq. (8), where the stress triaxiality, *T* is defined by the ratio of hydrostatic stress, σ_m and equivalent stress σ_e given by:

$$T = \frac{\sigma_m}{\sigma_e} = \frac{\sigma_1 + \sigma_2 + \sigma_3}{3\sigma_e}$$

(5)

$$\sigma_e = \frac{1}{\sqrt{2}} \left[(\sigma_1 - \sigma_2)^2 + (\sigma_3 - \sigma_1)^2 + (\sigma_2 - \sigma_3)^2 \right]^{\frac{1}{2}}$$

(6)

On the other hand, the equivalent strain ε_e is given by:

$$\sigma_e = \frac{\sqrt{2}}{2}\left[(\sigma_1 - \sigma_2)^2 + (\sigma_3 - \sigma_1)^2 + (\sigma_2 - \sigma_3)^2\right]^{\frac{1}{2}} \tag{7}$$

where the σ_1, σ_2, σ_3 and ε_1, ε_2, ε_3 are the principle stresses and principle strain, respectively. The fracture strain ε_f is determined using the equation proposed by Rice and Tracey [9]:

$$\varepsilon_f = A\,exp\left(-\frac{3}{2}\frac{\sigma_m}{\sigma_e}\right) \tag{8}$$

Where A is the material constant found through an experiment.

In the present work, the effect of corrosion defect on burst pressure was investigated through an experimental and numerical works. The burst pressure of defective pipes was predicted using a three-dimensional nonlinear, homogeneous isotropic elasto-plastic material model with large deformation finite element model. The SMCS model was used in predicting the failure of the defective pipe. The FE analysis results then were compared to available design codes for pipelines assessment with single longitudinal corrosion defects. The model was validated by comparing the FE results with physical testing and subsequently extensive parametric studies were carried out.

2. Material and Experimental Procedure

Tensile Test The material used in this study was API X42 steel. The chemical compositions and mechanical properties of the material are tabulated in Table 1 and Table 2, respectively.

Table 1. Chemical composition of API X42 steel (%wt)

C	P	Mn	S	Si	Fe	CE
0.03	0.01	0.98	0.003	0.19	98.6	0.21

Table 2. Mechanical properties of API X42 steel at room temperature

Young Modulus, E (GPa)	Yield Strength, σ_y (MPa)	Tensile Strength, σ_u (MPa)
207	284.7	464.4

The detailed specimen dimensions used for uniaxial tensile test are shown in Fig. 1. The test was performed according to ASTM E08-08 [14]. The specimens were extracted in longitudinal direction from API X42 steel pipes with schedule of 120. An extensometer with gauge length of 25 mm was attached to the specimen in order to monitor the axial displacement of the material. A total of four specimens were tested for a given geometry.
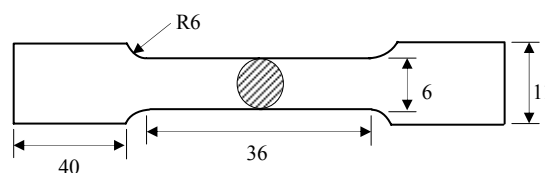
Figure 1. Smooth round tensile bar

Burst Pressure Test. Four API X42 steel pipes with different longitudinal artificial corrosion defect geometries were prepared. Detailed dimensions of the pipes with artificial corrosion defect are shown in Table 3. The defects on the pipe surface were machined using Computer Numerical Control (CNC) machine. The nominal outer diameter of the pipe is 60 mm. The overall length of the pipe was kept constant to be 600 mm. A schematic illustration of pipes with corrosion defect on its outer surface is shown in Fig. 2. The external thread with pitch of 2 mm was machined with 50 mm long on both ends of the defective pipes. The pipes were then attached to the cap with internal thread. The internal thread of the cap was machined with the same pitch of pipe thread. End of the pipes was sealed with aluminum O-rings to avoid leakage of the hydraulic oil when the pipes are pressurized. The cap has been covered by a solid cylinder to prevent the movement of the pipes in both transverse and longitudinal directions. Two solid cylinders were connected to each other using four threaded rods.

The defective pipe was internally pressurized by the oil using manual hydraulic pump. The pump was connected to the test rig through hydraulic line. Analog pressure gauge was attached between pump and defective pipe for pressure measurement. The oil was carefully pumped to the test rig to minimize the strain rate effect until the failure was detected on the pipe. During pressurization, the pipe was expanded and the localized bulge could be clearly seen in the weakest region. Detail experiment setup for the burst pressure testing is shown in Fig. 3a. The failure occurs on the principle plane direction. This is confirmed by observation on the failure pipe whereby the crack on defect is propagated in longitudinal direction. Figure 3b shows the API X42 steel pipe after performing the burst pressure test. The failure occurred at defective region where the minimum thickness of the pipe is placed. The maximum pressure which represents as the burst pressure was recorded and listed in Table 3.

Table 3. Effect of defect size on burst pressure

Case No.	Defect Dimension (mm)			Thickness, t (mm)	Burst Pressure (MPa)
	Length, l	Depth, d	Width, w		
EX1	49.7	4.1	13.7	5.80	54
EX2	49.8	3.5	13.9	5.60	61
EX3	69.7	4	17.3	5.55	46
EX4	50	4.5	14	5.62	44
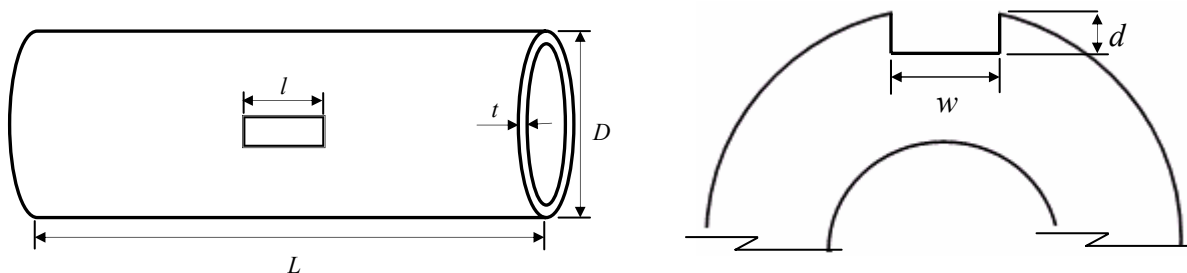
Figure 2. Schematic of pipes with corrosion defect
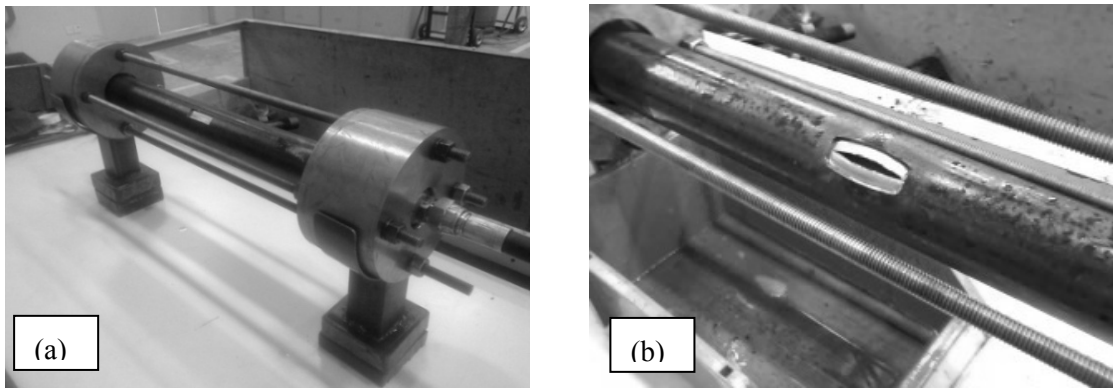
Figure 3. Experimental set up (a) Before Failure, (b) After Failure

3. Determination of SMCS Model Parameter

Remarking that the stress triaxiality for round bars is roughly $\sigma_m/\sigma_e \approx 1/3$. Substituting this value into Eq. (8), an approximate expression of the ratio of fracture strain ε_f is given by:

$$\frac{\varepsilon_f}{\varepsilon_f^*} = \frac{exp\left(\frac{-3\sigma_m}{2\sigma_e}\right)}{exp(-0.5)}$$

(9)

where ε_f^* denotes the fracture strain obtained from tensile test of smooth round bar. The value of average fracture strain is $\varepsilon_f^* = 1.04$ and is shown in Fig 7. Thus, the ε_f for API X42 material used in this paper is proposed to be:

$$\varepsilon_f = 1.732 exp\left(-1.5\frac{\sigma_m}{\sigma_e}\right)$$

(10)

Figure 4 shows the failure curve proposed for API X42 steel pipes based on Eq. (10).
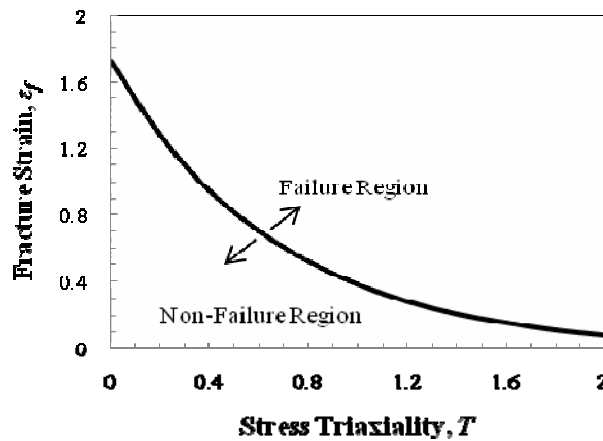
Figure 4. Failure curve for API X42 steel pipes

4. Validation of the Model

A 3-D nonlinear FE analysis was performed on experimental case studies listed in Table 3. The pipes with a rectangular artificial corrosion defects were modeled and eight node solid elements with reduced integration scheme are applied using commercial MSC PATRAN/MARC 2008r1 software. The material is modeled as an isotropic elasto-plastic material. Fig. 5 shows true stress strain data employed in FE analysis. The defective pipe with the same parameter used in experimental work was analyzed. A detailed finite element mesh applied on the models is shown in Fig. 6. Since the failure of the pipe was observed in defective region during the experiment, the FE mesh is designed sufficiently small around the defect area. The enlargement on the defective region is also shown in Fig. 6. Internal pressure was applied to the inner surface of the pipe. The boundary condition was applied at one end of the pipe to simulate the closed cap condition. The symmetrical condition was also applied for computational efficiency. The von Mises stress distribution on defect for pipe CS3 is shown in Fig. 7. At an applied pressure of 16 MPa, the pipe did not show any plastic deformation. However, at the onset of failure, the bulging on the defect can be clearly seen as shown in Fig. 7b. The reduction of pipe thickness at defective area was detected before the pipe started to burst.

To predict ductile failure of defective pipes made of API X42 steel pipes using the present approaches, the proposed Eq. (10) will be combined with detailed elasto-plastic FE analyses from which local stresses and strains are determined. For example, from the FE analysis, stress and strain data can be monitored as a function of pressure. Over the loading history, the stress triaxiality and equivalent strain were calculated using Eq. (5) to (7). Then, the equivalent strain to fracture or true fracture strain is estimated from Eq. (10). When the equivalent strain from the FE analysis equals to the fracture strain, failure is assumed to occur. The results of burst pressure from FE have been compared to experimental data and shown in Fig. 8. The percentage of the error for each case was also included. The maximum error between these two methods is 9%.
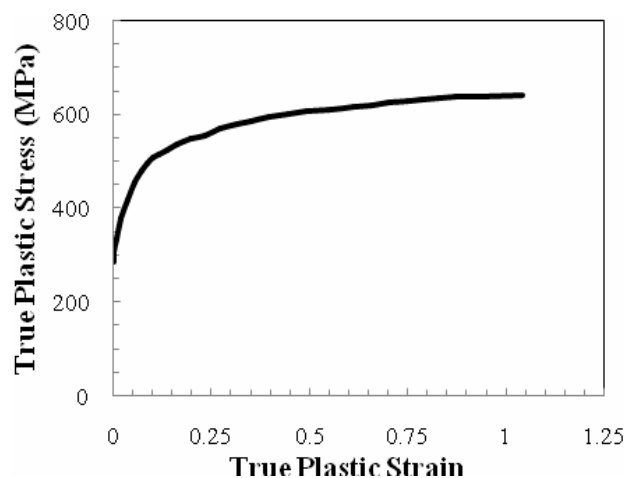
Figure 5. True plastic stress-strain data employed in FE analysis
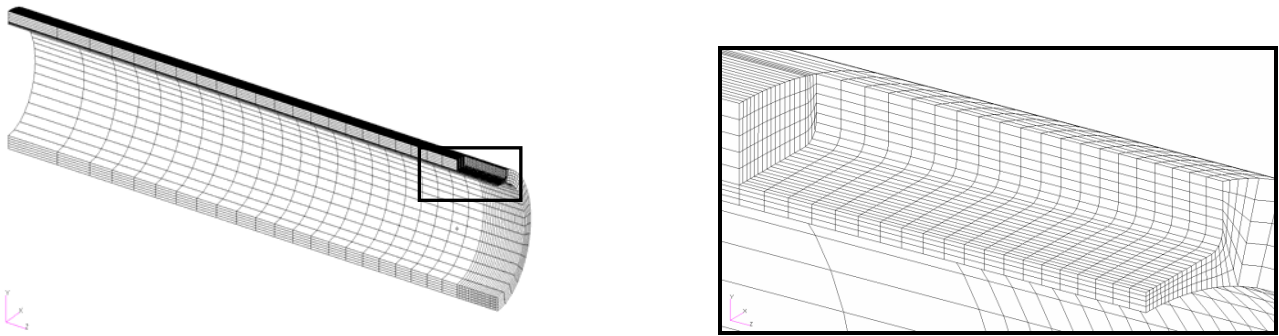
Figure 6. Detailed FE mesh of the model
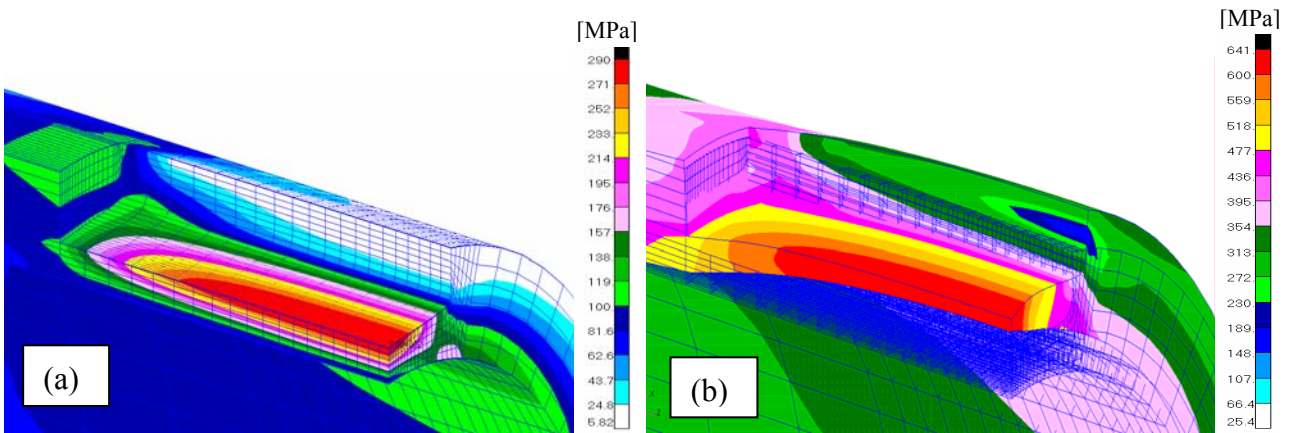
Figure 7. von Mises stress plots: (a) Internal pressure of 16 MPa, (b) Internal pressure of 64 MPa (Burst pressure)
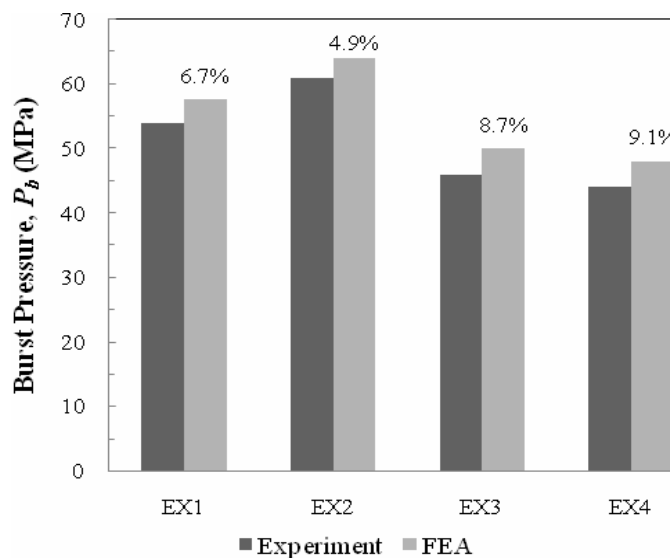
Figure 8. Comparison of burst pressure between experimental data and FE results

5. Parametric Study

The pipe with different defect depths, lengths and widths were simulated and the burst pressure for each case was predicted. In the present study, the totals of 10 cases represent by CS1 to CS10 were analyzed. The defect width, t depth, d and length, l for the case studies are summarized in Table 4. The wall thickness and outer diameter of the pipe are kept constant to be 6 mm and 60 mm, respectively.

Table 4. Different pipe sizes and defect dimensions

Case No.	Dimension (mm)			Failure Pressure (MPa)
	Length, l	Depth, d	Width, w	
CS1	50	3	14	83
CS2	50	3.5	14	72.4
CS3	50	4	14	64
CS4	50	4.5	14	52
CS5	50	3	10	83.2
CS6	50	3	6	84
CS7	50	3	4	84
CS8	30	3	14	88.4
CS9	40	3	14	86
CS10	60	3	14	81.6

Figure 9 shows the results of burst pressure predicted from FE analysis. The results of burst pressure calculated from ASME B31G, Modified ASME B31G and DNV-RP-F101 design codes for corroded pipelines were also included. Based on these three design codes, the failure of the pipelines is assume to occur when the stress developed in the pipes equal to or higher than the flow stress of the materials. Since the flow stress is always lower than the ultimate strength, the failure will be predicted before necking occurred. In contrast, SMCS model used in this paper predicted the failure based on the fracture strain of the materials. The parameter of the model is determined from fracture point during uniaxial tensile test, therefore necking of the material is allowed. Neglecting the increment of pressure from the onset of necking to fracture point causes the design codes to always give lower value in predicting the burst pressure. In general, the results of burst pressure calculated from these three design codes show lower values compared to FE. The results clearly show that ASME B31G design code gives lowest value of burst pressure in all cases studied. This is followed by modified ASME B31G and DNV-RP-F101 design codes except for cases CS3 and CS4 in which the modified ASME B31G appears as the most conservative compared to other codes. Referring to the FE results from Fig. 9a, the burst pressure slightly decreases as the length of defect increases from 30 mm to 60 mm. A similar pattern is shown by all design codes. In contrast, as the defect depths increase from 3 mm to 4.5 mm (50% to 75% of pipe thickness) as shown in Fig. 9b the burst pressure decreases significantly. The burst pressure drops higher than 13% as the depth of defect change even as small as 0.5 mm. In this respect, the defect depth appears as the main factor that governs the failure of the pipes. This observation is consistent with the fact that hoop stress is

dependent with the remaining effective thickness of the damage pipe as predicted in Eq. (1). The effect of defect width on burst pressure was also studied in this paper. Four different defect widths, w were simulated to investigate its effect on burst pressure. The results are summarized in Fig. 9c. Eq. (2) to Eq. (4) do not include the parameter, w. It is due to the assumption that the burst pressure is not affected by the width of the defect [4]. The assumption has been confirmed by the FE results in which as the width increases from 4 mm to 14 mm, almost no changes on burst pressure was detected.
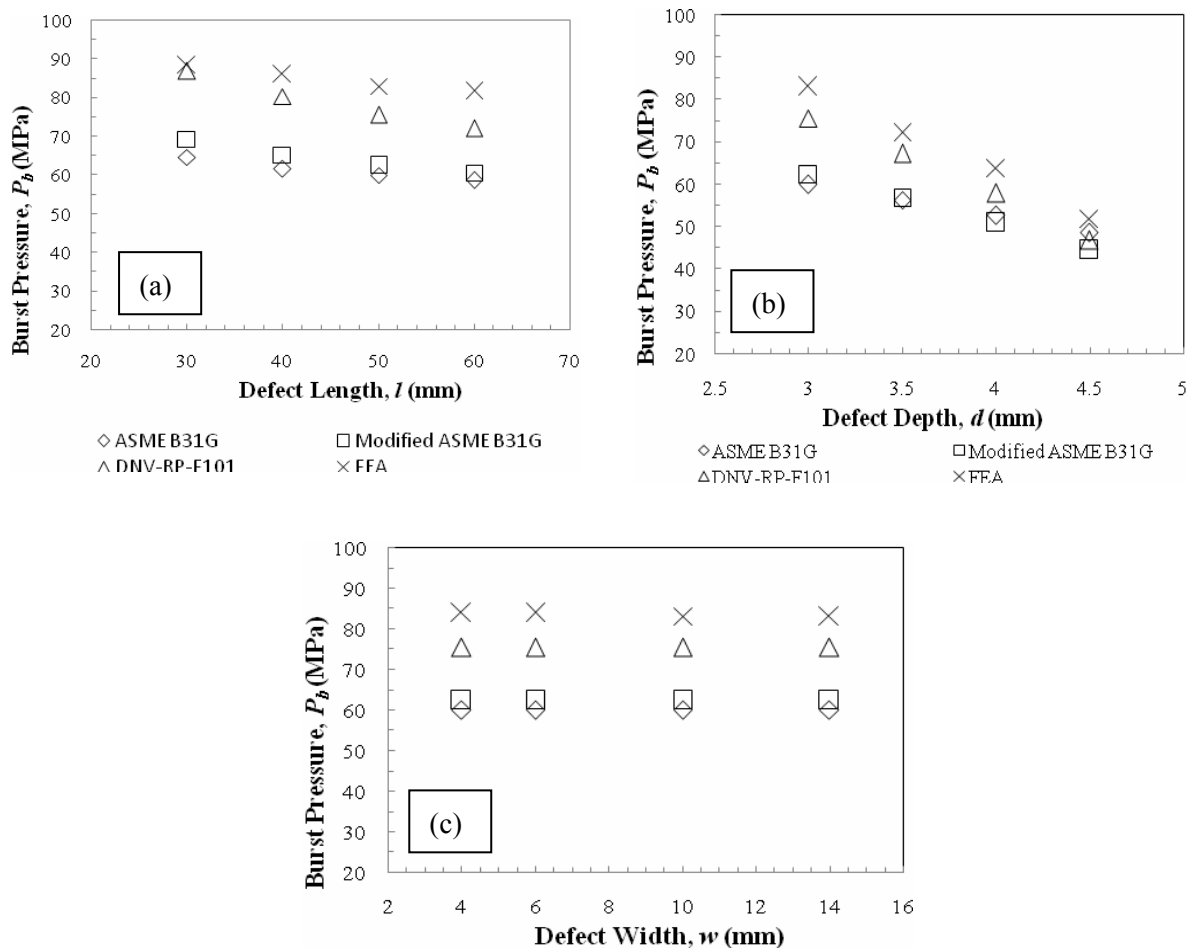
Figure 9. Effect on burst pressure (a) Defect length, (b) Defect depth, (c) Defect width

6. Conclusions

This paper has presented the effect of longitudinal corrosion defects on burst pressure of API X42 steel pipes. The results obtained are as follow:

1) The burst pressure of corroded pipelines is affected by the length and depth of the defects. The depth of corrosion defect is more influential parameter that would affect the burst pressure of pipes.

2) The width of the longitudinal corrosion defects affect insignificantly on burst pressure.

3) The FE results based on SMCS model always predict higher value of burst pressure compared to ASME B31G, Modified ASME B31G and DNV-RP-F101 design codes. ASME B31G is the most conservative design code.

Acknowledgments

References

[1] Y.K. Lee, Y.P. Kim, M.-W. Moon, 2005, The Prediction of Failure Pressure of Gas Pipeline with Multi Corroded Region, Materials Science Forum, 475-479, pp. 3323-3326

[2] ASME B31G-2009. Manual for Determining the Remaining Strength of Corroded Pipelines. A supplement to ASME B31 code for pressure piping. 2009.

[3] DNV Recommended Practice, RP-F101, 2010, Corroded pipelines, Det Norske Veritas.

[4] C.K. Oh, Y.J. Kim, J.H. Baek , W.-s. Kim, 2007, Ductile Failure Analysis of API X65 pipes with Notch-Type Defects using a Local Fracture Criterion, Int. J of Pressure Vessels and Piping 84, pp. 512–525

[5] Nasir Shafiq, Mokhtar Che Ismail, Chanyalew Taye, 2010, Burst Test Finite Element Analysis and Structural Integrity of Pipeline System, Hydrocarbon Asia's Engineering and Operations Convention. Kuala Lumpur, Malaysia

[6] T.A. Netto, U.S. Ferraz, S.F. Estefen, 2005, The Effect of Corrosion Defects on the Burst Pressure of Pipelines, Journal of Constructional Steel Research, 61, pp. 1185–1204

[7] L.Y. Xu, Y.F. Cheng, 2012, Reliability and Failure Pressure Prediction of Various Grades of Pipeline Steel in the Presence of Corrosion Defects and Pre-strain, International Journal of Pressure Vessels and Piping, 89, pp. 75-84

[8] A.L. Gurson, 1977, Continuum Theory of Ductile Rupture by Void Nucleation and Growth. Part 1-Yield Criteria and Flow Rules for Porous Ductile Media. J Eng Mater Tech, 1.

[9] J. R. Rice, D. Ai. Tracey, 1969, On the Ductile Enlargement of Voids In Triaxial Stress Fields, J. Mech. Phys. Solids, 17, pp. 201 -217.

[10] J.A Lemaitre, 1985, Continuous Damage Mechanics Model for Ductile Fracture, Journal of Engineering Material and Technology 107, pp.83-89

[11] J. W. Hancock and A.C. Mackenzie,1976, On The Mechanisms Of Ductile Failure In High-Strength Steels Subjected To Multi-Axial Stress-States, J. Mech. Phys. Solids, 24, pp. 147 - 169.

[12] C.K. Oh, Kim Y.J, J.H Baek , Y.P. Kim, W.-s. Kim, 2007, A phenomenological Model of Ductile Fracture for API X65 Steel, Int. Journal of Mechanical Sciences, 49, pp.1399-1412.

[13] C.K. Oh, Kim Y.J, Park JM, Baek JH, Kim WS.,2007, Development of Stress-Modified Fracture Strain for Ductile Failure of API X65 Steel, Int J Fract ,143,pp.119–33.

[14] ASTM Standard E8-08, 2008, Standard Test Method for Tension Testing of Metallic Material, American and Society for Testing and Materials.